Journal of Renewable Materials

Tech Science Press

DOI: 10.32604/jrm.2023.028877

ARTICLE

Biomass Carbon Improves the Adsorption Performance of Gangue-Based Ceramsites: Adsorption Kinetics and Mechanism Analysis

Haodong Li[1], Huiling Du[1,*], Le Kang[1], Yewen Zhang[1], Tong Lu[1], Yuchan Zhang[1], Lan Yang[2] and Shijie Song[2]

[1]College of Materials Science and Engineering, Xi'an University of Science and Technology, Xi'an, 710054, China

[2]Shccig Yulin Chemical Co., Ltd., Management Committee of Yushen Industrial Zone, Yulin, China

[*]Corresponding Author: Huiling Du. Email: hldu@xust.edu.cn

Received: 12 January 2023 Accepted: 15 March 2023 Published: 10 November 2023

ABSTRACT

The large accumulation of coal gangue, a common industrial solid waste, causes severe environmental problems, and green development strategies are required to transform this waste into high-value-added products. In this study, low-cost ceramsites adsorbents were prepared from waste gangue, silt coal, and peanut shells and applied to remove the organic dye methylene blue from wastewater. We investigated the microstructure of ceramsites and the effects of the sintering atmosphere, sintering temperature, and solution pH on their adsorption performance. The ceramsites sintered at 800°C under a nitrogen atmosphere exhibited the largest three-dimensional-interconnected hierarchical porous structure among the prepared ceramsites; further, it exhibited the highest methylene blue adsorption performance, with an adsorption capacity of 0.954 $mg{\cdot}g^{-1}$, adsorption efficiency of over 95%, and adsorption equilibrium time of 1 h at a solution pH of 9. The removal efficiency remained greater than 75% after five adsorption cycles. The adsorption kinetics data were analyzed using various models, including the pseudo-second-order kinetic model and Langmuir equation, and the adsorption was attributed to electrostatic interactions between the dyes and ceramsites, n-interactions, and hydrogen bonds. The prepared coal gangue ceramsites exhibited excellent adsorption capacities, removal rates, and cyclic stabilities, demonstrating their promising application prospects for the comprehensive utilization of solid waste and for wastewater treatment.

KEYWORDS

Porous ceramsites; adsorption; biological carbon; kinetic analysis; adsorption mechanism

1 Introduction

The generation of industrial solid waste has increased significantly owing to rising global industrialization. Comprehensively promoting the recycling of solid waste is an urgent requirement for green and sustainable development. Coal gangue is an industrial solid waste generated during coal mining and washing. According to a survey, approximately 60 billion tons of coal gangue are currently accumulated, and this amount is increasing at a rate of approximately 300 million tons per year [1,2]. In addition to occupying land resources, coal gangue buildup promotes spontaneous combustion and pollutes the atmosphere, seriously harming the environment and human health [3–5]. Therefore, many countries are concerned about reducing the accumulation of coal gangue and increasing its rate of

utilization [6–8]. Currently, the majority of coal gangue is used for land reclamation or for producing concrete, bricks, and cement. Gao et al. [9] analyzed the mechanical properties and durability of coal gangue concrete and its components. Zhou et al. [10] and Wu et al. [11] produced all-solid waste-based permeable bricks through a pressing–sintering process. However, additional innovative applications of coal gangue are required.

Coal gangue can be used as a raw material for ceramics because it mostly comprises SiO_2 and Al_2O_3, which fulfill the requirements for preparing ceramics [12,13]. Owing to their low heat conductivity, high porosity, large specific surface area, low bulk density, and stable chemical and physical properties, porous ceramics have been extensively studied for various applications [14]. The pore-forming agent method is widely used in the preparation of porous ceramics because of its simple preparation conditions, low cost, and relative environmental protection [15,16]. Xu et al. [17] used coal gangue, coal slime, and coconut palm fibers as raw materials to fabricate porous ceramics with a porosity of 66.930%, volume density of 1.033 $g{\cdot}cm^{-3}$, compressive strength of 1.103 MPa, and thermal conductivity of 0.392 $W{\cdot}m^{-1}{\cdot}K^{-1}$. Using a solid-phase sintering process, Hao et al. [18] fabricated a low-density ceramic proppant using calcined flint clay (45.6 wt% Al_2O_3) and solid-waste coal gangue. Sintering at 1400°C produced the best performing proppant with a bulk density of 1.270 $g{\cdot}cm^{-3}$, an apparent density of 2.790 $g{\cdot}cm^{-3}$, and breakage ratios of 3.270% and 8.360% at closed pressures of 35 and 52 MPa, respectively.

Organic dyes are used in numerous consumer products; for example, methylene blue (MB) and methyl orange are frequently used for dyeing textiles [19]. However, organic dye wastewater is harmful to aquatic life and humans. Organic dyes have been removed from wastewater using a variety of physicochemical techniques such as ion exchange, solvent extraction, electrochemical methods, adsorption, and photocatalysis [20–22]. Among these methods, adsorption is an effective technique for the treatment of organic wastewater. Recently, researchers prepared gangue-based adsorbents by exploiting the unique structure of gangue. Mohammadi et al. [23] modified coal gangue with iron oxide; the adsorption capacities of the modified coal gangue composite for Zn^{2+} and Mn^{2+} were 42.100 and 30.120 $mg{\cdot}g^{-1}$, respectively. Shang et al. [24] modified coal gangue with trimethoxysilane to adsorb Cd-(II), Hg-(II), and Pb-(II) from industrial waste. Xiong et al. [25] used zirconia-modified coal gangue to adsorb phenols and phosphates. Zhou et al. [26] created porous ceramic microspheres from waste gangue using a spray-drying technique and studied the adsorption kinetics, adsorption isotherms, and the effect of solution pH. The removal rates of the cationic red X-5GN and cationic blue X-GRR dyes were 1.044 and 2.170 $mg{\cdot}g^{-1}$, respectively. Yan et al. [27] prepared low-cost porous ceramic microspheres from waste gangue via simple spray drying and subsequent calcination. A 20 $g{\cdot}L^{-1}$ dose of microspheres calcined at 800°C removed 100% and 99.9% of MB and basic fuchsin, respectively, from wastewater. Chemically modifying gangue can increase the adsorption performance; however, modification is costly, and the chemical reagents can pollute the environment. Moreover, although the cost of porous ceramic microspheres is low, their pore structure and adsorption performance are limited, and they cannot be recovered after the adsorption test. Therefore, developing an absorbent that is low in cost, has high removal efficiency, and is easy to recover is critical.

In this study, porous ceramsites adsorbents were prepared from coal gangue and silt coal, using peanut shells as the pore-forming agent. No chemical modification of the ceramsites was required. The effects of the sintering atmosphere, sintering temperature, and pH level on the adsorption of organic dyes onto the porous ceramsites were systematically examined. The primary adsorption mechanisms were studied using adsorption kinetics, thermodynamics, and isothermal diagrams. A cyclic adsorption test was performed to demonstrate the practicability of the ceramsites. The use of peanut shells in the experiment not only provided a novel method for the treatment of agricultural waste but also increased the porosity of ceramsites, provided biochar, and enhanced its adsorption capacity.

2 Experimental

2.1 Materials

Raw coal gangue and silt coal were obtained from the Shendong mining area in Yulin City, Shaanxi Province, China. MB was supplied by Sinopharm Chemical Reagent Co., Ltd. (China). The MB concentration was determined from the linear relationship between the absorbance at 667 nm and the MB dye concentration: $y = 0.167x + 0.026$. The peanut shells were collected from local sources. Deionized water was used throughout the experimental processes.

The elemental compositions of the raw materials were determined using an X-ray fluorescence spectrometer, and the results are displayed in Table 1. The coal gangue primarily comprised SiO_2, Al_2O_3, and Fe_2O_3 and was used to prepare the ceramic materials. The silt coal was used as the adhesive.

Table 1: The chemical composition of raw materials (mass fraction, %)

Materials	SiO_2	Al_2O_3	Fe_2O_3	CaO	K_2O	Na_2O	MgO	Loss on ignition
Coal gangue	52.86	17.94	4.69	1.69	2.62	1.88	1.62	16.70
Silt coal	58.43	23.65	4.58	3.78	2.88	1.93	1.45	3.30

2.2 Preparation of Ceramic Adsorbents

The coal gangue porous ceramsites had been prepared by using a pore-forming agent and sintering; the fabrication procedure is shown in Fig. 1. First, the coal gangue and silt coal were ball-milled to fine powders with particle sizes of less than 0.075 mm (200 mesh). The coal gangue porous ceramsites were then prepared by mechanically mixing coal gangue powder, silt coal powder as the adhesive (10 wt%), peanut shell powder (10 wt%), and deionized water (15 wt%–20 wt%) for 2 h and aging for 24 h. Subsequently, the mixture was formed into balls (diameter [Φ]: 2–5 mm) using a granulating machine (QLC400-II, Chuzhou Huaye Electromechanical Co., China), and the samples were dried for 4 h in an oven at 100°C. Finally, the samples were sintered at 800°C, 900°C, or 1000°C in a tube furnace (GSL-1100X-S, Hefei Kejing Materials Technology Co., China) at a heating rate of 5°C·min^{-1} in an air or nitrogen atmosphere. The temperature was maintained for 2 h, followed by cooling to room temperature to form porous ceramsites. This method is suitable for the mass production of porous ceramsites.

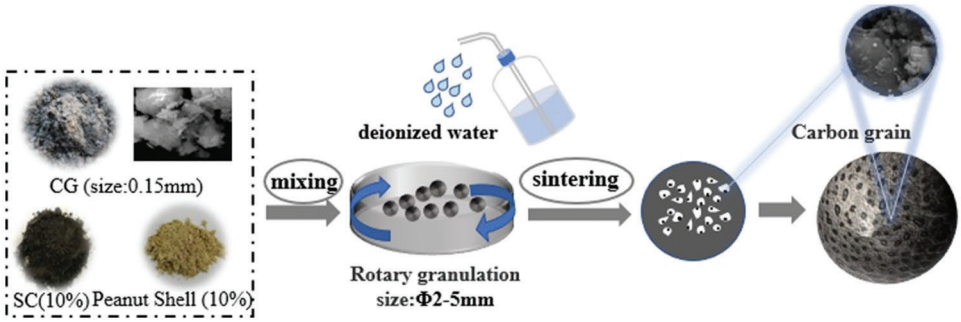

Figure 1: The preparation process of porous ceramsites

2.3 Characterization

An X-ray fluorescence spectrometer was used to determine the chemical composition of the raw coal gangue and silt coal powder (XRF; SPECTRO MIDEX, SPECTRO Analytical Instruments GmbH,

Germany). The phase compositions of the samples were examined using an X-ray powder diffractometer (XRD; XRD-6100X, Shimadzu Corporation, Japan). The functional groups of the adsorbents were examined both before and after the adsorption of organic dyes using a Fourier-transform infrared spectrometer (FT-IR; Nicolet IS5, Thermo Fisher Scientific, USA) in the 400–4000 cm^{-1} wavelength range. The surface appearance and microstructure of the materials were observed using a field-emission scanning electron microscope (FE-SEM; S-4800, Hitachi Corporation, Japan). The porosities of the samples were measured using the Archimedes method.

2.4 Adsorption Experiments

The effects of the sintering atmosphere, sintering temperature, and dyeing agent pH on the MB removal efficiency were investigated using adsorption tests. The absorbent (1 g) was added to a 20 $mg{\cdot}L^{-1}$ MB solution (50 mL) and magnetically stirred at 300 rpm for 1–5 h.

At 30-min intervals, samples of the supernatant were collected. After centrifugation, the solution concentration was calculated from the absorbance measured at 664 nm using an ultraviolet spectrophotometer [28]. The adsorption capacity and removal efficiency of the gangue ceramics for MB were calculated using Eqs. (1) and (2), respectively.

$$q_t = \frac{(C_0 - C_t)V}{m} \tag{1}$$

$$\eta = \frac{(C_0 - C_t)}{C_0} \times 100\% \tag{2}$$

where q_t ($mg{\cdot}g^{-1}$) is the adsorbed amount at time t, C_0 ($mg{\cdot}L^{-1}$) is the initial concentration of the dye, C_t ($mg{\cdot}L^{-1}$) is the concentration of the dye at time t, V (L) is the volume of the dye solution, m (g) is the dosage of the gangue adsorbent, and η (%) is the dye removal efficiency.

2.5 Adsorbent Regeneration Experiments

Based on the adsorption experiments, only the ceramsites sample with the highest adsorption capacity was used for the regeneration tests. The saturated adsorbent was dried and heated for 2 h at 500°C to induce MB decomposition. The samples were then reused for adsorption. Five regeneration cycles were performed.

2.6 Characterization of Coal Gangue Porous Ceramsites

Fig. 2 shows the XRD patterns of the coal gangue porous ceramsites. Quartz (SiO_2; JCPDS Card 46-1045) and kaolinite ($Al_4Si_4O_{10}(OH)_8$; JCPDS Card 14-0164) were the two major phases in coal gangue, as shown in Fig. 2a. It also contained illite ($(KH_3O)Al_2Si_3AlO_{10}(OH)_2$, JCPDS Card 02–0056). The phase of the coal gangue porous ceramsites was not noticeably altered as the sintering temperature increased from 800°C to 900°C. The kaolinite in the gangue decomposed above 500°C to produce amorphous metamorphic kaolin ($Al_2O_3{\cdot}2SiO_2$); however, after increasing the sintering temperature from 900°C to 1000°C, the metakaolin transformed into crystallized mullite, namely, $3(Al_2O_3{\cdot}2SiO_2) \rightarrow 3Al_2O_3{\cdot}2SiO_2 + 4SiO_2$. At this stage, a portion of the SiO_2 exhibited an amorphous crystal structure, as indicated by the corresponding decrease in the intensity of the crystalline silica diffraction peak [17]. The phase structure of the nitrogen-sintered ceramsites was similar to that of the air-sintered ceramsites, as shown in Fig. 2b.

The FT-IR spectra of the coal gangue ceramsites are shown in Fig. 2c. The bands at 3436 and 1633 cm^{-1} were assigned to the stretching and bending vibrations of surface–OH groups or water [29]. The 1076, 790, and 489 cm^{-1} peaks were attributed to the symmetric and antisymmetric Si–O–Si stretching vibrations, and the 559 cm^{-1} peak corresponded to the stretching vibration of Si–O–Al. Gangue ceramics contain many SiO_2

and Al_2O_3 tetrahedra and, because the silicon–oxygen bond is stronger than the aluminum–oxygen bond, the silico-aluminum isomorphous substitution may occur. The $Si–O^-$ exhibits a constant structural negative charge, which could encourage contact with the cationic dyes and improve the adsorption of cationic compounds by the ceramsites [27,30]. The various functional groups in the ceramsites provide many active sites, thus enhancing the adsorption performance.

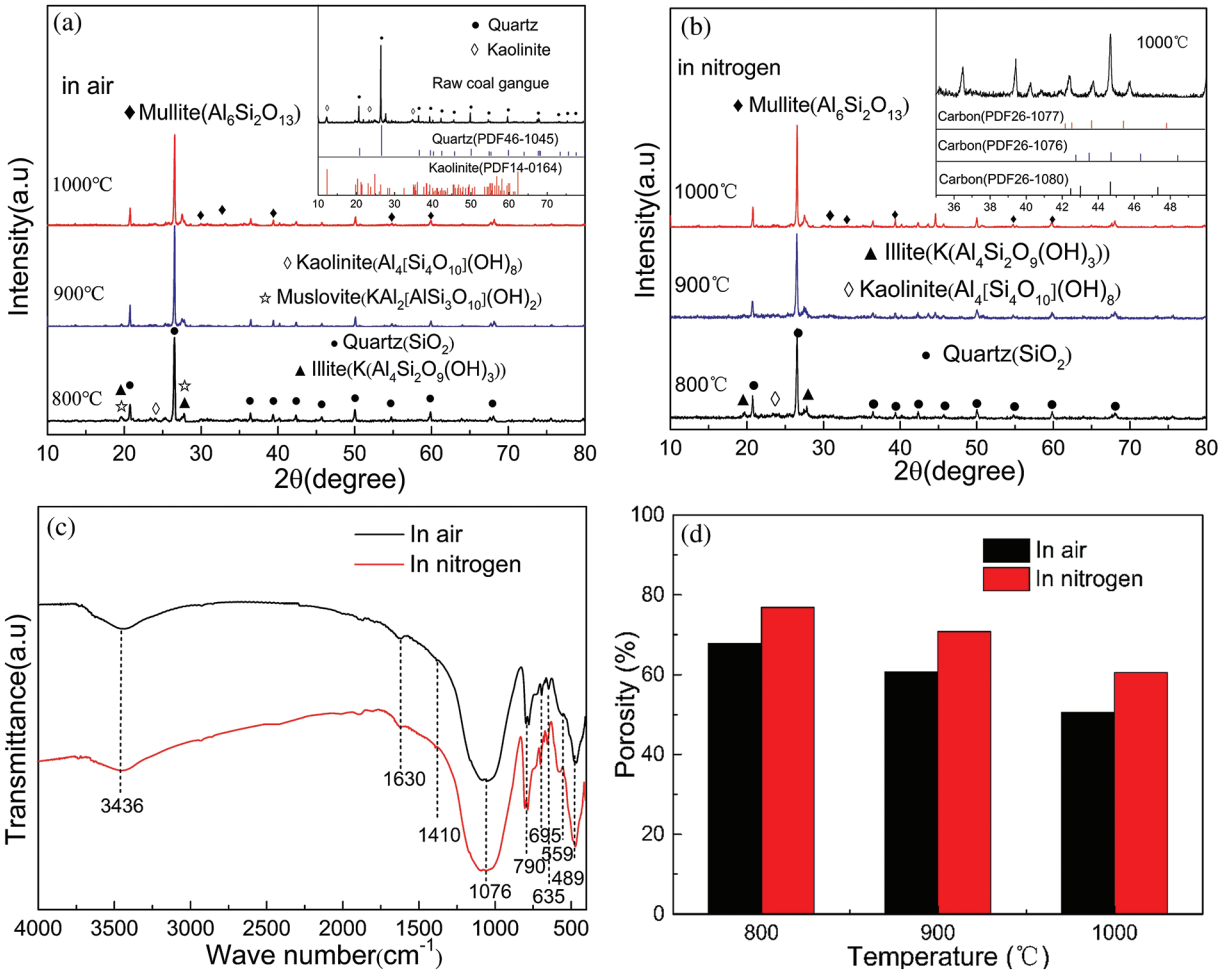

Figure 2: XRD pattern of porous ceramsites. (a) Sintering in air and (b) in nitrogen; (c) FTIR spectrum of ceramsites adsorbent, (d) effect of temperature on porosity

The porosity of the ceramsites was significantly affected by the sintering temperature. As shown in Fig. 2d, the porosity declined linearly with increasing sintering temperature. This may be because low-melting-point glass phases were produced; however, the primary reason was that linear shrinkage increased with increasing sintering temperature, decreasing porosity [31,32].

The interior three-dimensional (3D) porous microstructure of the ceramsites after sintering is shown in Fig. 3. The visible microscopic pores on the ceramsites surface acted as diffusion pathways for the adsorbates, improving the adsorption capacity. The microstructure of the ceramsites interior was extremely porous and as the sintering temperature increased, the interior became smooth. Furthermore, the inner part of the ceramsites retained the lamellar structure of kaolin, which agreed well with the XRD results. The nitrogen-sintered samples exhibited enhanced surface roughness compared to the air-sintered

samples, although the difference was insignificant. Furthermore, numerous ultrafine particles were attached to the ceramsites; however, whether these were biological carbon particles was unclear.

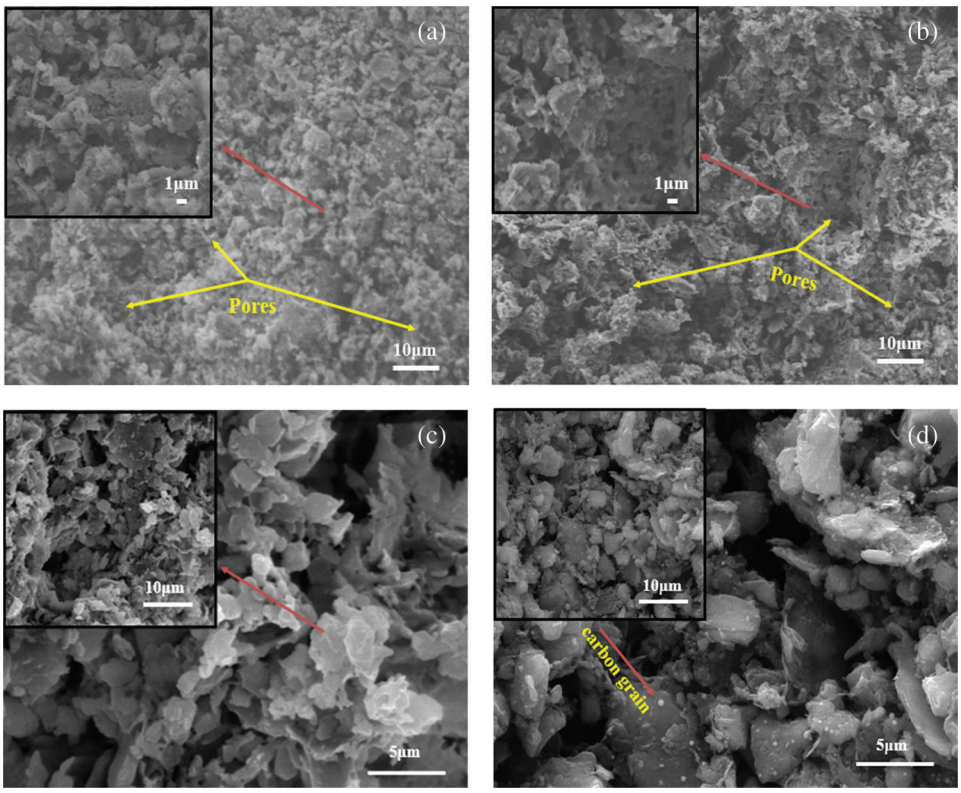

Figure 3: Cross sections of coal gangue ceramsites after treated at (a) 800°C, (b) 1000°C, (c) sintering in air, (d) sintering in nitrogen

2.7 Adsorption Properties

The sintering temperature of the ceramsites had a significant impact on MB adsorption, as illustrated in Figs. 4a and 4b. Compared to the ceramsites sintered at higher temperatures (900°C and 1000°C), the ceramsites sintered at 800°C exhibited enhanced adsorption properties and removal efficiency. The SEM images showed that as the sintering temperature increased, the porosity gradually decreased, the surface became smooth, and some components in the ceramsites melted, resulting in a liquid phase blocking the pores. This reduced the number of active sites, thus leading to a decrease in adsorption performance.

When the ceramsites were sintered in nitrogen instead of air, the adsorption performance and efficiency were enhanced because the peanut shells acted as a pore-forming agent and carbonized to generate biochar during nitrogen sintering. The hydroxyl groups on the surface of the carbon materials in the ceramsites served as active sites for chemical adsorption, thus improving the adsorption performance. The most notable improvement was observed for the ceramsites sintered at 900°C and 1000°C, which agreed well with the XRD and SEM results.

The pH of a solution affects the surface charge of the adsorbents; therefore, the pH of the organic dye is an important factor that influences the adsorption properties [33]. Figs. 4c and 4d show the effect of the waste liquid pH on the adsorption effectiveness. The highest MB adsorption efficiency was observed at a pH of ~9 under ambient experimental conditions, owing to the electrostatic interactions between the positively

charged cationic dyes and negatively charged anionic ceramsites. When the pH exceeded 9, the solution hydroxyl ions reacted with the ceramsites cations and occupied the active sites, which reduced the dye removal rate [34]. Because the biochar provided more active sites, the dye removal rate of the nitrogen-sintered ceramsites was higher than that of the air-sintered ceramsites.

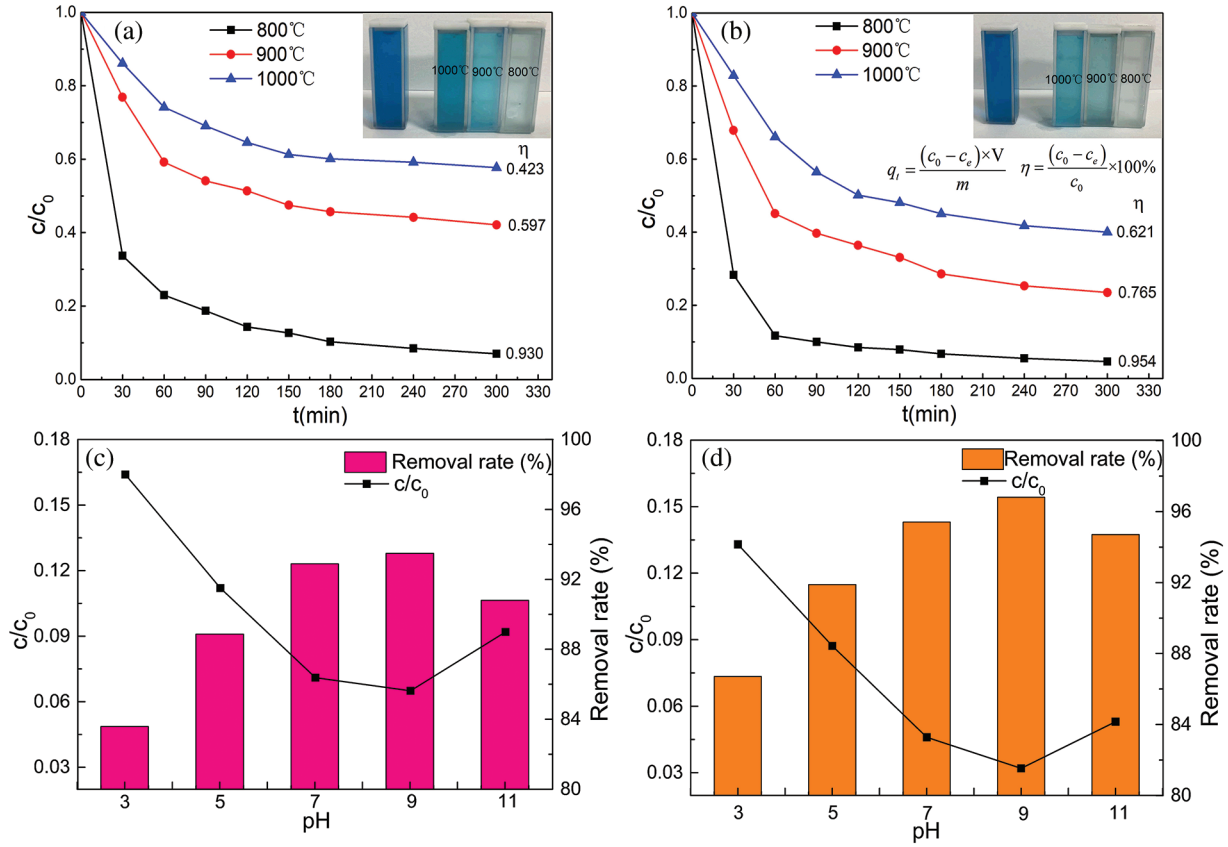

Figure 4: Effect of sinter temperature on MB adsorption performance and removal effectiveness. (a) Sintering in air and (b) in nitrogen; The ability of ceramsites to adsorb MB is affected by pH value. (c) Sintering in air, (d) sintering in nitrogen

2.8 Adsorption Kinetics and Isotherms

To further examine the adsorption process, the MB adsorption data were fitted to the pseudo-first-order, pseudo-second-order, intraparticle diffusion, and Elovich kinetic models [35]. The various fitted curves are shown in Figs. 5a–5d, and the fitting results are listed in Table 2. When the adsorption process reaches an equilibrium state, the adsorption isotherm, which depicts the distribution of the adsorbed molecules between the liquid and solid phases, can be used to assess the adsorption performance of a material. The MB adsorption isotherms of the ceramsites are shown in Figs. 5e and 5f. Two distinct isotherm models, Langmuir and Freundlich, were examined, where t (min) is the adsorption time, q_e ($mg{\cdot}g^{-1}$) and q_t ($mg{\cdot}g^{-1}$) are the adsorption capabilities of the ceramsites at time t and equilibrium, respectively, k_1 (min^{-1}) and k_2 ($mg^{-1}{\cdot}g^{-1}{\cdot}min^{-1}$) are the corresponding pseudo-first-order and second-order kinetic rate constants, respectively. k_i ($mg{\cdot}g^{-1}{\cdot}min^{-0.5}$) is the boundary layer constant and C ($mg{\cdot}g^{-1}$) is the intraparticle diffusion rate constant, which reflects the thickness of the boundary layer. α ($mg{\cdot}g^{-1}{\cdot}min^{-1}$) is the initial adsorption rate of the Elovich model, and β ($g{\cdot}mg^{-1}$) is the Elovich model constant.

c_e (mg L^{-1}) is the equilibrium concentration of the adsorbate in solution, q_e (mg·g^{-1}) and q_{max} (mg·g^{-1}) are the adsorption capacities at equilibrium and the maximum monolayer adsorption capacities, respectively, K_L (L·mg^{-1}) and K_F (L·mg^{-1}) are the Langmuir and Freundlich constants, respectively, which represent the adsorption energy, and n is the Freundlich intensity factor.

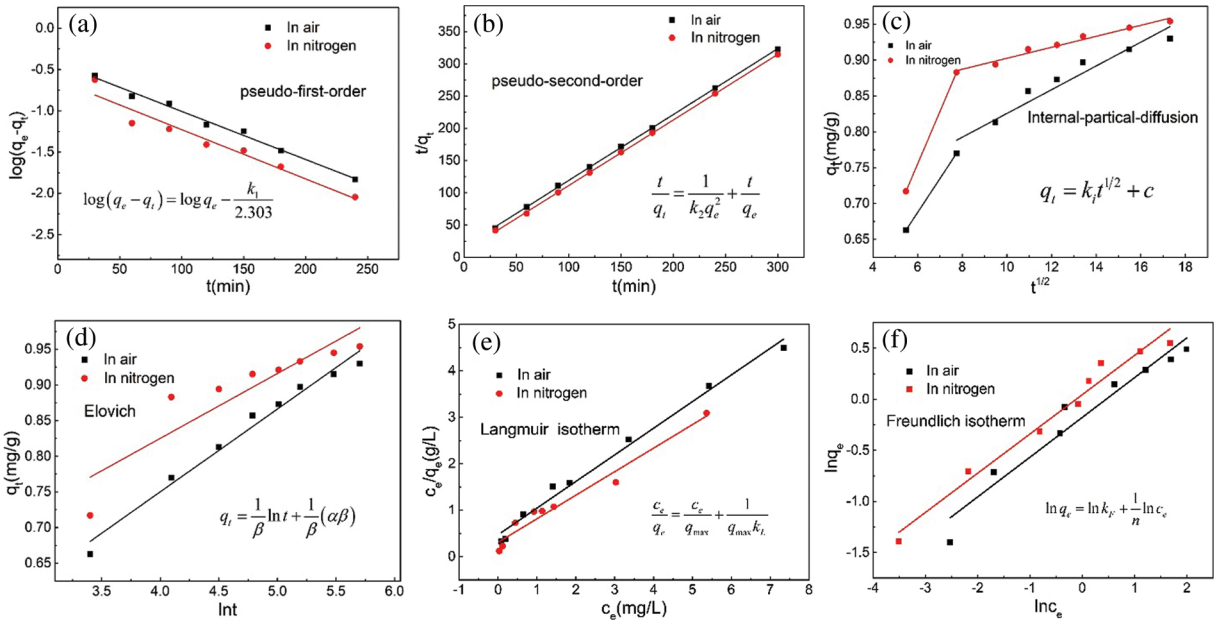

Figure 5: Kinetic fits for MB adsorption. (a) Pseudo-first-order, (b) pseudo-second-order, (c) intra-particle diffusion and (d) elovich model; Isotherms fits for MB adsorption. (e) Langmuir, (f) freundlich

Table 2: Kinetics model fitting parameters for the adsorption of MB by the ceramsites

	Parameters	In air	In nitrogen
Pseudo-first-order	k_1 (min^{-1})	0.013	0.014
	q_e (mg·g^{-1})	0.377	0.235
	R^2	0.983	0.930
Pseudo-second-order	k_2 (mg^{-1}·g^{-1}·min^{-1})	0.062	0.112
	q_e (mg·g^{-1})	0.977	0.982
	R^2	0.997	0.999
Intraparticle diffusion	K_{i1}	0.379	0.028
	K_{i2}	0.010	0.009
	C_1	0.694	0.793
	C_2	0.660	0.826
	R_1^2	0.966	0.946
	R_2^2	0.898	0.919
Elovich	α	1.356	29.211
	β	8.609	11.918
	R^2	0.976	0.970

The pseudo-second-order kinetics model fitting had the highest R^2 value among the various models, indicating that this model better reflected the process of MB adsorption by the ceramsites. This suggested that the adsorption process was chemical in nature and was primarily governed by electrostatic contact and electron transfer between the adsorbent and adsorbate [36]. In addition, the adsorption data were well fitted by the intraparticle diffusion model. The adsorption curves indicated that there were two steps in the adsorption process. (I) Instantaneous adsorption stage: the "liquid membrane" above the ceramsites surface allowed MB molecules in the solution to reach the surface. (II) Internal diffusion stage: The inner composition and pore size of the ceramsites were the main limiting factors. The R^2 of the internal diffusion model for sintering in nitrogen was closer to 1 than that of sintering in air (Table 2). This may be because the peanut shell biochar produced during sintering in nitrogen affected the internal structure and pore characteristics of the ceramsites. Internal diffusion was not the only regulating element, as indicated by the linear trend that did not pass through the origin [37,38].

The parameters for the fitting of the adsorption isotherm results are listed in Table 3. The sorption of the air-sintered ceramsites shown in Fig. 5e was better fitted to the Langmuir isotherm ($R^2 = 0.964$). Monolayer adsorption accounted for the majority of MB adsorption on the ceramsites. In nitrogen-sintered systems, the Freundlich and Langmuir isotherms adequately described the adsorption, with R^2 values of 0.959 and 0.970, respectively, indicating that multilayer adsorption may occur based on monolayer adsorption [39]. The maximum adsorption capacities of the two adsorbents were 1.492 and 1.974 $mg{\cdot}g^{-1}$, respectively.

Table 3: Isotherm parameters for the adsorption of MB by the ceramsites

	Parameters	In air	In nitrogen
Langmuir isotherm	k_L ($L{\cdot}mg^{-1}$)	1.322	1.645
	q_{max} ($mg{\cdot}g^{-1}$)	1.492	1.974
	R^2	0.964	0.959
Freundlich isotherm	k_F ($L{\cdot}mg^{-1}$)	0.837	1.046
	1/n	0.384	0.389
	R^2	0.937	0.970

As shown in Table 4, in order to check the adsorption capacity of competitive adsorbents for organic dyes, the adsorption capacity of the gangue-based porous ceramsite synthesized in this study was compared with that of different gangue-based materials and other organic dyes adsorbents reported in the literature. The organic dye adsorption capacity of the synthesized gangue-based porous ceramsites sieve was similar to or exceeded that of other adsorbents reported in the literature. An additional benefit of our material is the ease of recycling after adsorption.

Table 4: Comparison of dyes adsorption capacity of different adsorbents

Adsorbents	Dye	q_{max} ($mg{\cdot}g^{-1}$)	Reference
Gangue ceramic microbeads	Cationic blue X-GRRL	0.918	[26]
Modified pumice stone	Methylene blue	15.870	[40]
Moroccan illite	Methylene blue	13.600	[41]
ZFA/HZ	Methylene blue	45.090	[42]
Kenaf fiber char	Methylene blue	22.700	[43]
Gangue-based ceramsites	Methylene blue	0.954	Present work

2.9 Adsorption Mechanism and Recyclability

Recycling spent adsorbents must be considered while assessing their quality and cost. Because organic dyes can be easily decomposed in kaolinite at high temperatures, cyclic testing was performed by calcining the ceramsites at 500°C for 2 h to remove the organic dyes.

Fig. 6a shows that the ceramsites adsorption still performed well, and the removal efficiency remained greater than 75% after five adsorption cycles. This demonstrates that the ceramsites adsorbent can be reused for several MB adsorption cycles, which is a significant advantage over powdered adsorbents. However, a slight reduction in adsorption capacity was observed after multiple cycles because multiple calcinations of ceramsites can alter the functional groups and lead to pore collapse, which reduces the number of active sites and specific surface area, and eventually lowers the adsorption ability of the adsorbent. Both types of ceramsites exhibit excellent cyclic regeneration and provide significant economic benefits.

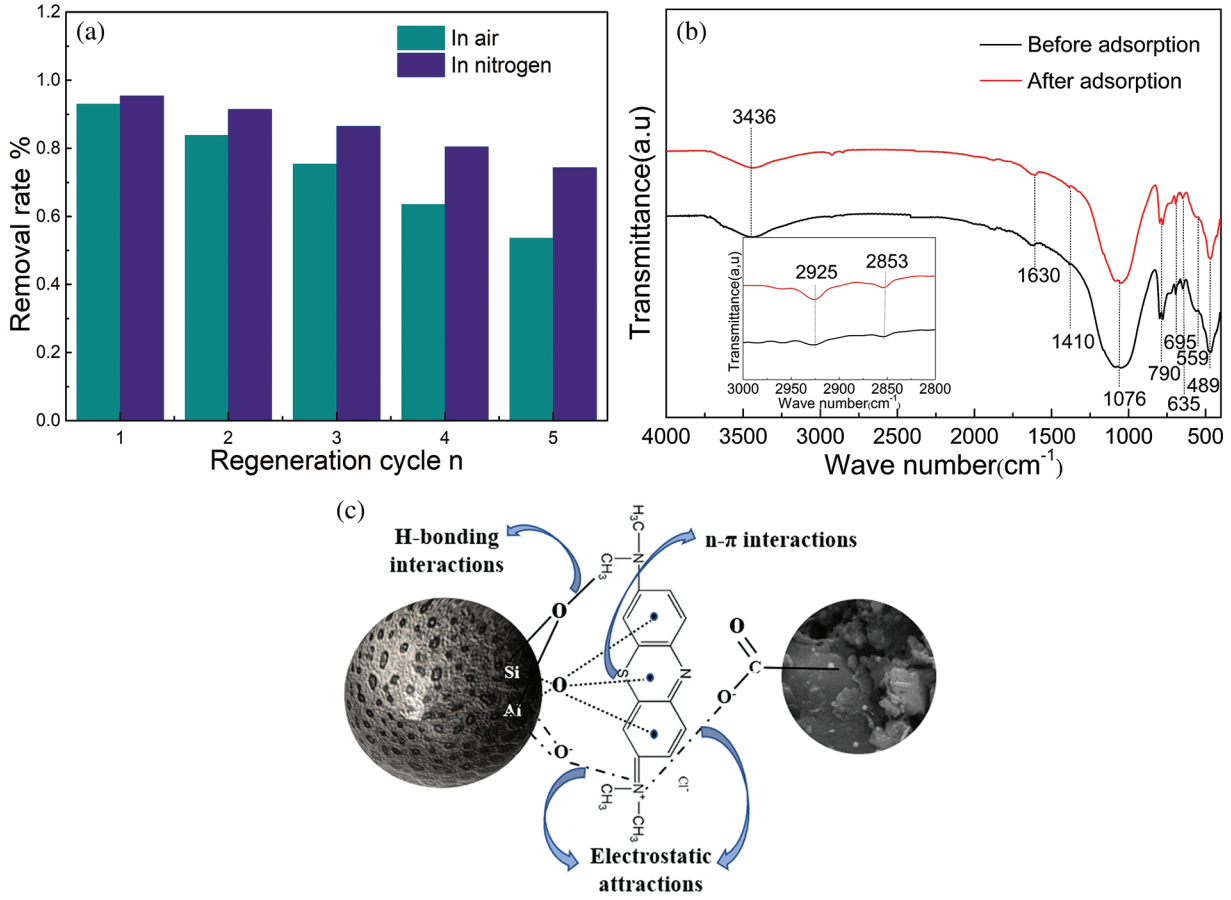

Figure 6: (a) Regeneration properties of the ceramsites and (b) FTIR spectra of the ceramsites before, after MB adsorption, (c) adsorption mechanism

As shown in Fig. 6b, significant differences were observed in the FT-IR spectra of the ceramsites before and after adsorption of MB. The bands centered at 2925 and 2853 cm^{-1} corresponded to the stretching vibrations of aromatic rings, and those at 1410 cm^{-1} corresponded to the bending vibration of methylene, clearly indicating MB adsorption [44].

The basic characterization of the ceramsites, adsorption performance tests, and isothermal and kinetic model-fitting results was used to determine the probable adsorption mechanism depicted in Fig. 6c. The

ceramsites surface contains many adsorption sites, including silico-aluminum groups and hydroxyl (–OH) groups on the mineral edges that provide surface negative charges that interact with the dyes. In addition, the O lone-pair electrons delocalize into the π orbitals of the dye aromatic rings to form n-π bonds, and the H of the surface hydroxyl groups forms an H-bond with the N in the MB dye structure [45,46]. Furthermore, the nitrogen-sintered ceramsites contain biocarbon, which can provide abundant functional groups (C–H, C=C, C=O, and C–C) that bind to MB to improve the adsorption performance [47,48].

3 Conclusions

In this study, highly porous ceramsites were fabricated using peanut shells, coal gangue, and coal slime. The following conclusions were obtained:

1. The 3D-interconnected porous structure of the ceramsites provided more active sites that benefited the attachment of the adsorbate. Therefore, compared with sintering in air, the MB removal efficiency was improved when the ceramsites were sintered in nitrogen, with increased removal efficiencies observed for ceramsites sintered at low temperatures. The maximum adsorption capacity and removal efficiency of 0.954 $mg \cdot g^{-1}$ and 96%, respectively, were observed at a sintering temperature of 800°C.
2. MB adsorption onto ceramsites followed the pseudo-second-order kinetic model and the Langmuir equation. The primary adsorption process involves hydrogen bonding and electrostatic interactions between the dyes and ceramsites. The removal efficiency remained greater than 75% after five adsorption cycles.
3. This research offers a new application for coal gangue and silt coal and an effective method to remove organic dyes from wastewater. In addition, the dye-adsorbed ceramsites can be used as ceramic waste, which is an advantage over powdered adsorbents. However, to reduce secondary pollution, the leachability of ceramsites adsorbents must be reduced, which will be the focus of future studies.

Funding Statement: This work was supported by the Natural Science Foundation of China under Grant (No. 52172099) and the Provincial Joint Fund of Shaanxi (2021JLM-28).

Author Contributions: The authors confirm contribution to the paper as follows: study conception and design: Li Haodong, Du Huiling; data collection: Li Haodong, Kang Le; analysis and interpretation of results: Li Haodong, Kang Le, Zhang Yewen; draft manuscript preparation: Lu Tong, Zhang Yuchan, Yang Lan, Song Shijie. All authors reviewed the results and approved the final version of the manuscript.

Conflicts of Interest: The authors declare that they have no conflicts of interest to report regarding the present study.

References

1. Zhang, Y. L., Ling, T. C. (2020). Reactivity activation of waste coal gangue and its impact on the properties of cement-based materials—A review. *Construction and Building Materials, 234,* 117424. https://doi.org/10.1016/j.conbuildmat.2019.117424
2. Li, J. Y., Wang, J. M. (2019). Comprehensive utilization and environmental risks of coal gangue: A review. *Journal of Cleaner Production, 239,* 117946. https://doi.org/10.1016/j.jclepro.2019.117946
3. Li, L. X., Zhang, Y. M., Zhang, Y. F., Sun, J. M., Hao, Z. F. (2016). The thermal activation process of coal gangue selected from Zhungeer in China. *Journal of Thermal Analysis and Calorimetry, 126(3),* 1559–1566. https://doi.org/10.1007/s10973-016-5711-4
4. Jablonska, B., Kityk, A. V., Busch, M., Huber, P. (2017). The structural and surface properties of natural and modified coal gangue. *Journal of Environmental Management, 190(3),* 80–90. https://doi.org/10.1016/j.jenvman.2016.12.055

5. Kong, N., Du, H. L., Li, Z., Lu, T., Xia, S. Y. et al. (2023). Nano heterojunction of double MOFs for improved CO_2 photocatalytic reduction performance. *Colloids and Surfaces A: Physicochemical and Engineering Aspects, 663,* 131005. https://doi.org/10.1016/j.colsurfa.2023.131005
6. Li, S. Q., Liber, K. (2018). Influence of different revegetation choices on plant community and soil development nine years after initial planting on a reclaimed coal gob pile in the Shanxi mining area, China. *Science of the Total Environment, 618(6),* 1314–1323. https://doi.org/10.1016/j.scitotenv.2017.09.252
7. Zhang, M., Liu, Y., Li, D., Cui, X., Wang, L. et al. (2023). Electrochemical impedance spectroscopy: A new chapter in the fast and accurate estimation of the state of health for lithium-ion batteries. *Energies, 16(4),* 1599. https://doi.org/10.3390/en16041599
8. Zhang, M., Wang, W. L., Xia, G. T., Wang, L. C., Wang, K. (2023). Self-powered electronic skin for remote human-machine synchronization. *ACS Applied Electronic Materials, 5(1),* 498–508. https://doi.org/10.1021/acsaelm.2c01476
9. Gao, S., Zhang, S. M., Guo, L. H. (2021). Application of coal gangue as a coarse aggregate in green concrete production: A review. *Materials, 14(22),* 6803. https://doi.org/10.3390/ma14226803
10. Zhou, W. F., Du, H. L., Kang, L., Du, X., Shi, Y. P. et al. (2022). Microstructure evolution and improved permeability of ceramic waste-based bricks. *Materials, 15(3),* 1130. https://doi.org/10.3390/ma15031130
11. Wu, C. L., Jiang, W., Zhang, C., Li, J. W., Wu, S. et al. (2022). Preparation of solid-waste-based pervious concrete for pavement: A two-stage utilization approach of coal gangue. *Construction and Building Materials, 319,* 125962. https://doi.org/10.1016/j.conbuildmat.2021.125962
12. Li, Z., Li, X., Tang, Y., Liu, T., Wu, T. et al. (2016). Sintering behaviour and characterisation of low-cost ceramic foams from coal gangue and waste quartz sand. *Advances in Applied Ceramics, 115(7),* 377–383. https://doi.org/10.1080/17436753.2016.1161692
13. Ran, H. P., Du, H. L., Ma, C. Y., Zhao, Y. Y., Feng, D. N. et al. (2021). Effects of A/B-site co-doping on microstructure and dielectric thermal stability of $AgNbO_3$ ceramics. *Science of Advanced Materials, 13(5),* 741–747. https://doi.org/10.1166/sam.2021.3943
14. Feng, D. N., Du, H. L., Ran, H. P., Lu, T., Xia, S. Y. et al. (2022). Antiferroelectric stability and energy storage properties of co-doped $AgNbO_3$ ceramics. *Journal of Solid State Chemistry, 310,* 123081. https://doi.org/10.1016/j.jssc.2022.123081
15. Li, T. P., Sun, T. T., Li, D. X. (2018). Preparation, sintering behavior, and expansion performance of ceramsite filter media from dewatered sewage sludge, coal fly ash, and river sediment. *Journal of Material Cycles and Waste Management, 20,* 71–79. https://doi.org/10.1007/s10163-016-0547-3
16. Li, T. P., Fan, J., Sun, T. T. (2020). Acid red G dye removal from aqueous solutions by porous ceramsite produced from solid wastes: Batch and fixed-bed studies. *Green Processing and Synthesis, 9(1),* 770–782. https://doi.org/10.1515/gps-2020-0068
17. Xu, H., Du, H. L., Kang, L., Cheng, Q. D., Feng, D. N. et al. (2021). Constructing straight pores and improving mechanical properties of gangue-based porous ceramics. *Journal of Renewable Materials, 9(12),* 2129–2141. https://doi.org/10.32604/jrm.2021.016090
18. Hao, J., Hao, H., Gao, Y., Li, X., Qin, M. et al. (2019). Effect of sintering temperature on property of low-density ceramic proppant adding coal gangue. *Materials Science, 26(1),* 94–98. https://doi.org/10.5755/j01.ms.26.1.19376
19. Chen, G. D., Feng, J., Wang, W. S., Yin, Y. D., Liu, H. Z. (2017). Photocatalytic removal of hexavalent chromium by newly designed and highly reductive TiO_2 nanocrystals. *Water Research, 108(6),* 383–390. https://doi.org/10.1016/j.watres.2016.11.013
20. Mouni, L., Belkhiri, L., Bollinger, J. C., Bouzaza, A., Assadi, A. et al. (2018). Removal of methylene blue from aqueous solutions by adsorption on kaolin: Kinetic and equilibrium studies. *Applied Clay Science, 153,* 38–45. https://doi.org/10.1016/j.clay.2017.11.034
21. Kundu, S., Chowdhury, I. H., Naskar, M. K. (2019). Hierarchical porous carbon nanospheres for efficient removal of toxic organic water contaminants of phenol and methylene blue. *Journal of Chemical and Engineering Data, 64(3),* 559–573. https://doi.org/10.1021/acs.jced.7b00745

22. Zhang, Y. W., Du, H. L., Lu, J., Li, Z., Lu, T. et al. (2023). Enhanced cyclic stability of Ga_2O_3@PDA-C nanospheres as pseudocapacitive anode materials for lithium-ion batteries. *Fuel, 334,* 126683. https://doi.org/10.1016/j.fuel.2022.126683
23. Mohammadi, R., Azadmehr, A., Maghsoudi, A. (2020). Enhancing of competitive adsorptive removal of zinc and manganese from aqueous solution by iron oxide-combusted coal gangue composite. *Separation Science and Technology, 55(18),* 3343–3361. https://doi.org/10.1080/01496395.2019.1706570
24. Shang, Z. B., Zhang, L. W., Zhao, X. Y., Liu, S. H., Li, D. L. (2019). Removal of Pb(II), Cd(II) and Hg(II) from aqueous solution by mercapto-modified coal gangue. *Journal of Environmental Management, 231,* 391–396. https://doi.org/10.1016/j.jenvman.2018.10.072
25. Xiong, J. B., Zang, L., Zha, J. F., Mahmood, Q., He, Z. L. (2019). Phosphate removal from secondary effluents using coal gangue loaded with zirconium oxide. *Sustainability, 11(9),* 2453. https://doi.org/10.3390/su11092453
26. Zhou, L., Zhou, H. J., Hu, Y. X., Yan, S., Yang, J. L. (2019). Adsorption removal of cationic dyes from aqueous solutions using ceramic adsorbents prepared from industrial waste coal gangue. *Journal of Environmental Management, 234,* 245–252. https://doi.org/10.1016/j.jenvman.2019.01.009
27. Yan, S., Pan, Y. M., Wang, L., Liu, J. J., Zhang, Z. J. et al. (2018). Synthesis of low-cost porous ceramic microspheres from waste gangue for dye adsorption. *Journal of Advanced Ceramics, 7(1),* 30–40. https://doi.org/10.1007/s40145-017-0253-1
28. Rahman, K. H., Kar, A. K. (2020). Effect of band gap variation and sensitization process of polyaniline (PANI)-TiO_2 p-n heterojunction photocatalysts on the enhancement of photocatalytic degradation of toxic methylene blue with UV irradiation. *Journal of Environmental Chemical Engineering, 8(5),* 104181. https://doi.org/10.1016/j.jece.2020.104181
29. Yin, Y., Xu, G. Y., Li, L. L., Xu, Y. X., Zhang, Y. H. et al. (2020). Fabrication of ceramsite adsorbent from industrial wastes for the removal of phosphorus from aqueous solutions. *Journal of Chemistry, 2020,* 8036961. https://doi.org/10.1155/2020/8036961
30. Nandi, B. K., Goswami, A., Das, A. K., Mondal, B., Purkait, M. K. (2008). Kinetic and equilibrium studies on the adsorption of crystal violet dye using kaolin as an adsorbent. *Separation Science and Technology, 43(6),* 1382–1403. https://doi.org/10.1080/01496390701885331
31. Pillai, U., Heider, Y., Markert, B. (2018). A diffusive dynamic brittle fracture model for heterogeneous solids and porous materials with implementation using a user-element subroutine. *Computational Materials Science, 153(5),* 36–47. https://doi.org/10.1016/j.commatsci.2018.06.024
32. Sun, Z., Fan, J., Yuan, F. (2015). Three-dimensional porous silica ceramics with tailored uniform pores: Prepared by inactive spheres. *Journal of the European Ceramic Society, 35(13),* 3559–3566. https://doi.org/10.1016/j.jeurceramsoc.2015.06.020
33. Yin, Y., Xu, G. Y., Li, L. L., Qiao, C. L., Xiao, Y. H. et al. (2021). Removal of inorganic arsenic from aqueous solution by Fe-modified ceramsite: Batch studies and remediation trials. *Water Science and Technology, 83(7),* 1522–1534. https://doi.org/10.2166/wst.2021.076
34. Shishkin, A., Aguedal, H., Goel, G., Peculevica, J., Newport, D. et al. (2021). Influence of waste glass in the foaming process of open cell porous ceramic as filtration media for industrial wastewater. *Journal of Cleaner Production, 282,* 124546. https://doi.org/10.1016/j.jclepro.2020.124546
35. Hassan, A. F., Elhadidy, H. (2017). Production of activated carbons from waste carpets and its application in methylene blue adsorption: Kinetic and thermodynamic studies. *Journal of Environmental Chemical Engineering, 5(1),* 955–963. https://doi.org/10.1016/j.jece.2017.01.003
36. Chang, W., Zhang, L., Qin, J., Zhang, P. F., Fu, C. Y. et al. (2022). Chestnut-shell-derived magnetic porous carbon for removing malachite green dye from water. *Journal of Chemical Engineering of Japan, 55(1),* 1–7. https://doi.org/10.1252/jcej.21we024
37. Yuan, N., Cai, H., Liu, T., Huang, Q., Zhang, X. L. (2019). Adsorptive removal of methylene blue from aqueous solution using coal fly ash-derived mesoporous silica material. *Adsorption Science & Technology, 37(3–4),* 333–348. https://doi.org/10.1177/0263617419827438

38. Sun, X. F., Ma, L. Q., Ye, G. C., Wu, L., Li, J. H. et al. (2021). Phenol adsorption kinetics and isotherms on coal: Effect of particle size. *Energy Sources Part A: Recovery Utilization and Environmental Effects, 43(4),* 461–474. https://doi.org/10.1080/15567036.2019.1628130
39. Gong, G. Q., Liang, S. J., Shi, Y. M., Wang, Z. Y., Li, Z. L. et al. (2022). Preparation of microporous carbon materials using residual coal from oxidative degradation of lignite as the carbon source and the mechanism and dynamics of its methyl orange adsorption. *Colloids and Surfaces A: Physicochemical and Engineering Aspects, 636(4),* 128138. https://doi.org/10.1016/j.colsurfa.2021.128138
40. Derakhshan, Z., Baghapour, M. A., Ranjbar, M., Faramarzian, M. (2013). Adsorption of methylene blue dye from aqueous solutions by modified pumice stone: Kinetics and equilibrium studies. *Health Scope, 2(3),* 136–144.
41. Amrhar, O., Nassali, H., Elyoubi, M. S. (2015). Adsorption of a cationic dye, methylene blue, onto moroccan illitic clay. *Journal of Materials and Environmental Science, 6(11),* 3054–3065.
42. Lin, L. D., Lin, Y., Li, C. J., Wu, D. Y., Kong, H. N. (2016). Synthesis of zeolite/hydrous metal oxide composites from coal fly ash as efficient adsorbents for removal of methylene blue from water. *International Journal of Mineral Processing, 148,* 32–40. https://doi.org/10.1016/j.minpro.2016.01.010
43. Mahmoud, D. K., Salleh, M. A. M., Karim, W. A. W. A., Idris, A., Abidin, Z. Z. (2012). Batch adsorption of basic dye using acid treated kenaf fibre char: Equilibrium, kinetic and thermodynamic studies. *Chemical Engineering Journal, 181,* 449–457. https://doi.org/10.1016/j.cej.2011.11.116
44. Novais, R. M., Carvalheiras, J., Tobaldi, D. M., Seabra, M. P., Pullar, R. C. et al. (2019). Synthesis of porous biomass fly ash-based geopolymer spheres for efficient removal of methylene blue from wastewaters. *Journal of Cleaner Production, 207,* 350–362. https://doi.org/10.1016/j.jclepro.2018.09.265
45. AL-Shehri, H. S., Alanazi, H. S., Shaykhayn, A. M., ALharbi, L. S., Alnafaei, W. S. et al. (2022). Adsorption of methylene blue by biosorption on alkali-treated solanum incanum: Isotherms, equilibrium and mechanism. *Sustainability, 14(5),* 2644. https://doi.org/10.3390/su14052644
46. Scheufele, F. B., Staudt, J., Ueda, M. H., Ribeiro, C., Steffen, V. et al. (2020). Biosorption of direct black dye by cassava root husks: Kinetics, equilibrium, thermodynamics and mechanism assessment. *Journal of Environmental Chemical Engineering, 8(2),* 103533. https://doi.org/10.1016/j.jece.2019.103533
47. Fan, S., Tang, J., Wang, Y., Li, H., Zhang, H. et al. (2016). Biochar prepared from co-pyrolysis of municipal sewage sludge and tea waste for the adsorption of methylene blue from aqueous solutions: Kinetics, isotherm, thermodynamic and mechanism. *Journal of Molecular Liquids, 220,* 432–441. https://doi.org/10.1016/j.molliq.2016.04.107
48. Guo, C., Zou, J., Yang, J., Wang, K., Song, S. (2020). Surface characterization of maize-straw-derived biochar and their sorption mechanism for Pb^{2+} and methylene blue. *PLoS One, 15(8),* e0238105. https://doi.org/10.1371/journal.pone.0238105